Theoretical and Experimental Studies on the Visible Light Activity of TiO₂ Modified with Halide-Based Ionic Liquids

Marta Paszkiewicz-Gawron [1,2,*]**, Samanta Makurat** [3] **, Janusz Rak** [3]**, Magdalena Zdrowowicz** [3]**, Wojciech Lisowski** [4]**, Adriana Zaleska-Medynska** [1]**, Ewa Kowalska** [2]**, Paweł Mazierski** [1] **and Justyna Łuczak** [5,*]

[1] Department of Environmetal Technology, Faculty of Chemistry, University of Gdańsk, Wita Stwosza 63, 80-308 Gdańsk, Poland; adriana.zaleska-medynska@ug.edu.pl (A.Z.-M.); pawel.mazierski@ug.edu.pl (P.M.)
[2] Institute for Catalysis, Hokkaido University, Sapporo 001-0021, Japan; kowalska@cat.hokudai.ac.jp
[3] Laboratory of Biological Sensitizers, Faculty of Chemistry, University of Gdańsk, Wita Stwosza 63, 80-308 Gdańsk, Poland; samanta.makurat@ug.edu.pl (S.M.); janusz.rak@ug.edu.pl (J.R.); magdalena.zdrowowicz@ug.edu.pl (M.Z.)
[4] Institute of Physical Chemistry Polish Academy of Science, 01-244 Warsaw, Poland; wlisowski@ichf.edu.pl
[5] Department of Process Engineering and Chemical Technology, Chemical Faculty, Gdańsk Univeristy of Technology, Narutowicza 11/12, 80-233 Gdańsk, Poland
[*] Correspondence: m.paszkiewicz-gawron@ug.edu.pl (M.P.-G.); justyna.luczak@pg.edu.pl (J.Ł.); Tel.: +48-58-523-52-22 (M.P.-G.); +48-58-347-13-65 (J.Ł.)

check for updates

Abstract: Formation of a surface complex between organic molecules and TiO₂ is one of the possible strategies for the development of visible light-induced TiO₂ photoactivity. Herein, three ionic liquids (ILs) with the same cation and different anions (1-butylpirydynium chloride/bromide/iodide) have been applied for the surface modification of TiO₂ and to understand the role of anions in visible light-induced activity of ILs-TiO₂ systems. Photocatalytic screening tests (the measurements of phenol photodegradation reaction rate) revealed that anion type affected visible light activity ($\lambda > 420$ nm) of TiO₂ obtained by the ILs-assisted solvothermal method. Density functional theory (DFT) calculations demonstrated that interactions between halogen anions and oxygen vacancies (OV) on the surface of the TiO₂ particles could be responsible for the specific wavelength-induced excitation and finally for the observed photoactivity of titania under visible light. Finally, our theoretical calculations have been proven by experiments using monochromatic light (the apparent quantum efficiency was measured) and the properties of obtained samples were characterized using scanning electron microscopy (SEM), X-ray powder diffraction analysis (XRD), UV-Vis spectroscopy and X-ray photoelectron spectroscopy (XPS).

Keywords: ionic liquids; apparent quantum efficiency; photocatalysis; DFT model; titanium dioxide; anions

1. Introduction

Semiconductor photocatalysis, with a dominant role of TiO₂ as a representative catalyst, was, up to date, applied to a variety of environmental and energy problems. However, since titania absorbs wavelengths shorter than 400 nm (due to the large band gap), its practical application requires usage of UV irradiation sources. In this regard, a lot of effort was made to design and tailor physical, chemical and optical properties of TiO₂ to extend its absorption to the visible range. Various strategies, such as surface photosensitization [1], doping with heteroatoms [2], charge transfer (CT)

interaction [3], coupling with a narrow band gap semiconductors [4] and modification with noble metals [5] were employed to utilize a larger fraction of the solar spectrum in the processes involving the TiO$_2$ photocatalyst.

Another, actually unexpected, way to improve TiO$_2$ photoactivity under visible irradiation turned out to be application of ionic liquids (ILs) for the preparation of TiO$_2$ microparticles [6]. These salts, with melting point below 100 °C, are usually composed of organic, asymmetric cations, and organic or inorganic anions. In contrary to other liquids, ILs are formed of supramolecular network of ions interacting via Coulombic forces, dipole−dipole and π–π interactions, hydrogen bonds, etc. [7,8]. These interactions, also present between IL moieties and titania precursor, affect size and surface architecture of TiO$_2$ nano- and microparticles surrounded by the IL's protective layer, which in turn, modify titania photoreactivity [8,9].

In this regard, a controllable preparation of the functional TiO$_2$ semiconductor employing ionic liquids is a new and effective approach [10,11]. Nevertheless, the mechanism of IL action and their role in the TiO$_2$ photoactivity enhancement have not been fully explained yet. Application of various IL-assisted strategies to obtain the IL-TiO$_2$ composites and characteristics of these materials revealed that ILs could improve the Vis response of this wide-band-gap semiconductor by: (i) doping of the crystalline structure with nonmetal elements (e.g., N, B, F) [12]; (ii) favoring oxygen vacancies (OV) and Ti^{3+} species formation on the titania surface [13]; (iii) forming surface complex charge transfer [14] and (iv) affecting transport of photogenerated charges [15]. Moreover, new energy levels can be formed between TiO$_2$, being an n-type semiconductor, and the halogen anion of IL [16]. In addition, the mechanism of the IL-TiO$_2$ photoactivity is strictly dependent on the IL structure and its thermal stability (due to possible thermal decomposition of IL under synthesis conditions) [16].

The aim of this work is to further explain the mechanism of phenol photodegradation mediated by the IL-TiO$_2$ microparticles, which were prepared in the presence of three halide-based 1-butylpirydynium ionic liquids ([BPy][X]; [X]: Cl$^-$, Br$^-$, I$^-$). The theoretical model has been confirmed by experiments using monochromatic light.

2. Results

Application of 1-butylpirydynium ionic liquids ([BPy][X]; where [X] is Cl$^-$, Br$^-$ or I$^-$) was dictated by the observation that 1-butylpirydynium chloride used for TiO$_2$ preparation provided photocatalyst with tremendous visible light driven activity [16]. Therefore, in this study, TiO$_2$ was synthesized by the solvothermal method in the presence of [BPy][X] containing chloride, bromide or iodide anions (Figure 1).
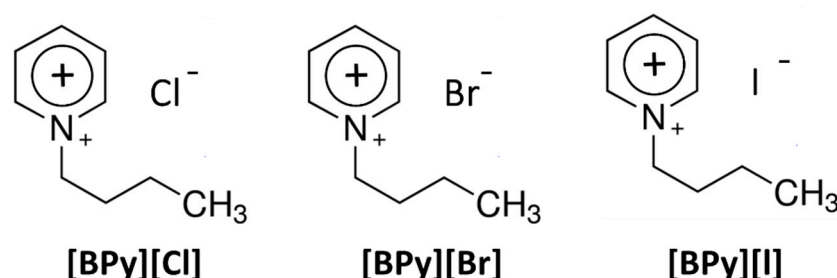

Figure 1. The structure of 1-butylpirydynium: chloride/bromide/iodide ionic liquids.

2.1. Structure, Morphology and Optical Properties

To give more information about the IL-TiO$_2$ photocatalysts used in this study basic material characteristics was performed. As shown in Figure 2, the X-ray diffraction analysis was applied to verify the crystalline phase of the obtained samples. A set of diffraction peaks at 2θ values near 25.3°, 37.7°, 48°, 54°, 55°, 63° and 68.5° were observed for all samples, which are attributed to the anatase phase formation. The analysis confirmed that the samples do not contain any impurities and anatase

phase with high quality was formed. Ionic liquids addition did not cause any changes in the crystal structure of the obtained samples.
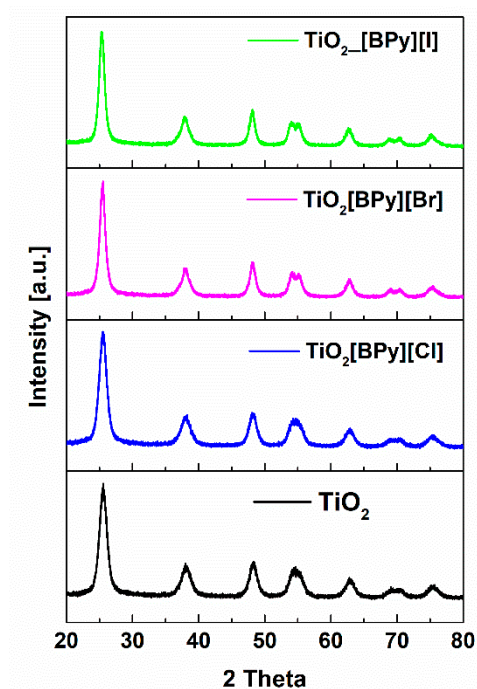

Figure 2. The X-ray diffraction patterns for the IL-TiO$_2$ and pristine TiO$_2$ samples.

The surface morphology and microstructure of the reference TiO$_2$ and IL-TiO$_2$ samples were characterized by SEM (Figure 3). It was demonstrated that pristine TiO$_2$ as well as modified TiO$_2$ had a spherical shape. For the samples prepared with addition of ionic liquids the dominant fraction were microparticles with average diameter from 1 to 2 µm, while in the case of reference TiO$_2$, the largest contribution was particles with sizes 3–5 µm. Moreover, the microspheres of pristine TiO$_2$ were more irregular in size and shape, compared to IL-assisted TiO$_2$ samples. As it shown in Figure 3, the microparticles prepared with addition of ILs had smoother surface and more uniform particle size distribution. The average size of the microspheres was calculated based on the statistical size of at least one hundred particles in the case of each sample. It was revealed that samples TiO$_2$_[BPy][Cl], TiO$_2$_[BPy][Br] and TiO$_2$_[BPy][I] yielded mainly microparticles with diameter of 1–3 µm, with the highest contribution of 1–2 µm, in an amount of 70%, 45% and 58%, respectively. The percentage contribution of large particles, with diameter 3–5 µm was rarely reached for ILs-assisted samples and never exceeded 16%, however for the pristine TiO$_2$ the amount of this fraction was 52%. The formation of the microspheres probably started with hydrolysis of the TBOT precursor, followed by the formation and growth of the TiO$_2$ crystallites (nucleation). The XRD measurements (see Table S1) revealed that the average diameter, as well as, volume of crystallites of the IL-TiO$_2$ photocatalysts were higher than that detected for pristine TiO$_2$. These dimensions increased in the following order TiO$_2$_[BPy][Cl] < TiO$_2$_[BPy][Br] < TiO$_2$_[BPy][I]. In the next step, the crystallites aggregated to create the spherical shape of the particles. Some small crystallites may detach from the particle surface and diffuse into solution because of the tendency to reduce the overall energy of the particle, which is called the Ostwald ripening mechanism. This mechanism is also related with the deposition of smaller particles on the larger crystals [17]. ILs as surface active agents may adsorb at the particle surface forming the surface layer, thereby limiting smaller particles deposition during Ostwald ripening, inhibiting further growth and agglomeration [10,16]. Growth of the particles is usually a diffusion-limited process, therefore a structure and content of the ionic liquid used in the reaction system influence TiO$_2$ particles' growth [10,16,18]. Further, as shown in Figure 3, more uniform particle size distribution in case of the

IL-TiO$_2$ microparticles was probably also due to steric hindrance and ability of the alkyl substituents to take a variety of arrangements.
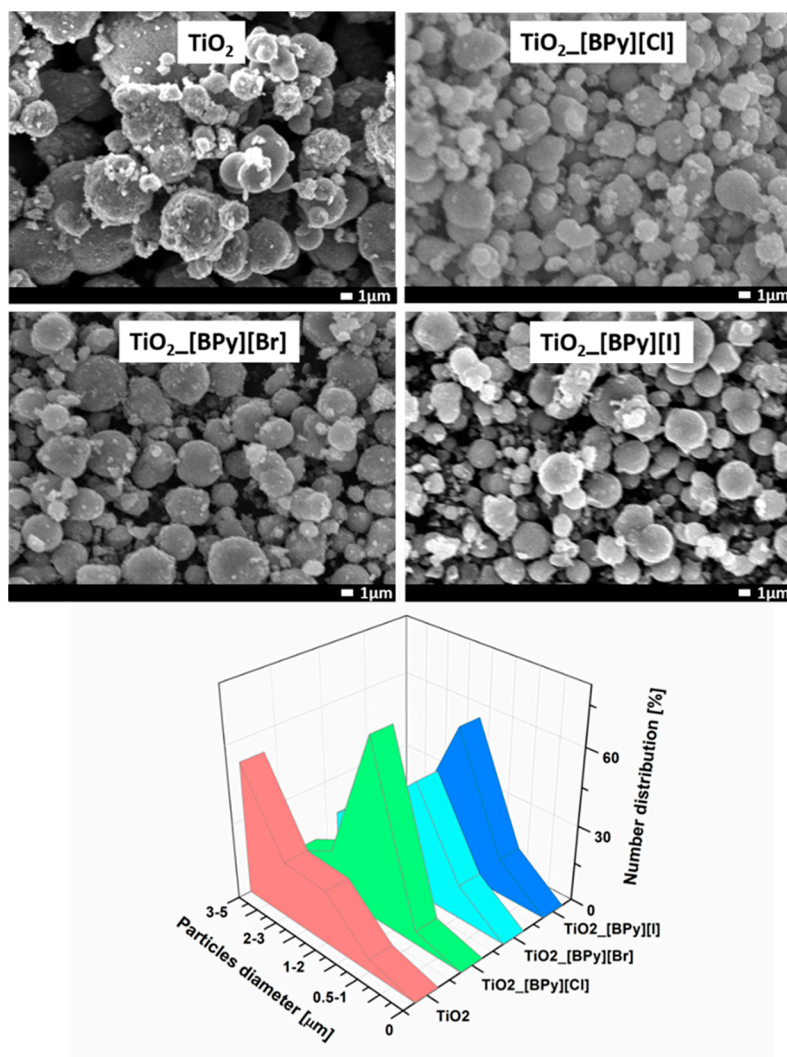

Figure 3. SEM images and particle size distribution of TiO$_2$ obtained by solvothermal process: without IL, with [BPy][Cl], [BPy][Br] and [BPy][I] ionic liquids.

The UV-Vis absorption spectra of the photocatalysts prepared with addition of different ILs as well as pristine TiO$_2$ are presented in Figure 4. Pristine TiO$_2$ absorbed irradiation mainly in the UV range ($\lambda < 400$ nm). Addition of ionic liquids to the reaction environment resulted in noticeably increased absorption in the visible irradiation range ($\lambda > 400$ nm) when compared with pristine TiO$_2$. Moreover, depending on the type of added ionic liquid, absorption differed in the visible light range. Generally, the enhancement of Vis light absorption was in the following order: TiO$_2$_[BPy][Cl] > TiO$_2$_[BPy][Br] > TiO$_2$_[BPy][I].

The Ti 2p XPS spectra revealed the signals attributed to Ti3+ species to increase for IL-assisted samples, which, in turn, indicate a higher content of oxygen vacancies (see Table 1, Figure S1) in the halogen-based ILs-TiO$_2$ particles. For example, for the TiO$_2$_[BPy][Cl] sample, the amount of Ti^{3+} states was 7.36 at.% while that for pristine TiO2 only 2.41 at.%. This finding prompted us to hypothesize that oxygen vacancies could play a basic role in the mechanism of excitation of IL-TiO$_2$ under visible irradiation, which will be discussed in the next section of this article. Moreover, the XPS results demonstrate that IL anions form a protecting layer surrounding the TiO$_2$ particle as a result of interaction with the TiO$_2$ surface (see Table S2). It was revealed that C–Nx bonds were present in the

IL-modified TiO$_2$ samples. Additionally, the presence of individual elements (Cl, Br, I) on the surface of the IL-TiO$_2$ samples was confirmed (Table S2).
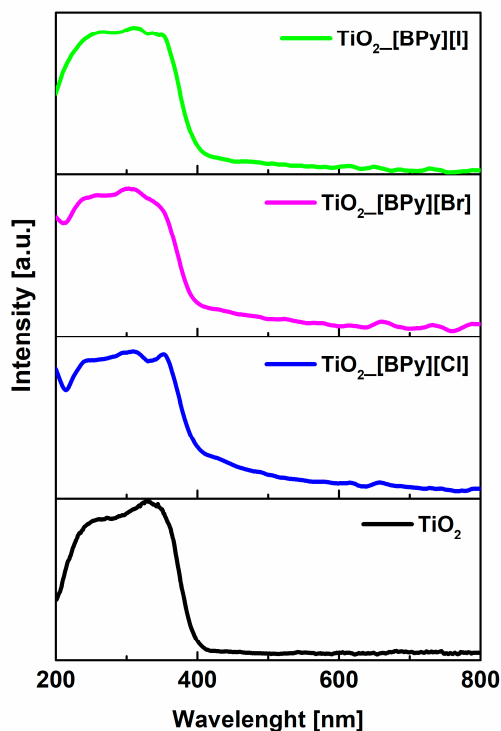

Figure 4. UV-Vis absorption spectra of pristine TiO$_2$ and TiO$_2$ obtained using ionic liquid containing various anions.

Table 1. Elemental composition (in at. %) and chemical characters of titanium states in the surface layer of and the samples: TiO$_2$_[BPy][Cl], TiO$_2$_[BPy][Br], TiO$_2$_[BPy][l].

Sample	Ti 2p$_{3/2}$ Fraction (%)		
	$\sum$ Ti (at.%)	Ti^{4+} 458.7 $\pm$ 0.3 eV (%)	Ti^{3+} 457 $\pm$ 0.3 eV (%)
TiO$_2$	29.44	97.59	2.41
TiO$_2$_[BPy][Cl]	24.58	92.64	7.36
TiO$_2$_[BPy][Br]	25.67	95.86	4.14
TiO$_2$_[BPy][I]	24.79	95.92	4.08

2.2. Photocatalytic Activity and Mechanism

Firstly, as a screening test, the photocatalytic activity of the TiO$_2$_[BPy][X] composites analyzed for wavelengths longer that 420 nm (visible range of irradiation – optical filter λ > 420 nm) was found to follow the order: TiO$_2$_[BPy][Br] > TiO$_2$_[BPy][I] > TiO$_2$_[BPy][Cl] (Table 2 and Figure S2). At this stage, it was revealed that addition of ionic liquid to the reaction environment caused increased photocatalytic activity, as shown based on the photodegradation reaction rate, in comparison to pristine TiO$_2$ (prepared in the same way but without ILs).

Table 2. Phenol degradation reaction rates under visible irradiation for the samples: TiO$_2$, TiO$_2$_[BPy][Cl], TiO$_2$_[BPy][I], TiO$_2$_[BPy][Br] (screening tests).

Sample	Phenol Degradation Reaction Rate under UV-Vis Irradiation λ > 420 nm (μmol·dm^{-3}·min^{-1})
TiO$_2$	0.22
TiO$_2$_[BPy][Cl]	0.87
TiO$_2$_[BPy][I]	0.96
TiO$_2$_[BPy][Br]	1.19

To explain the effect of the anion type on the TiO$_2$_[BPy][X] photoactivity we proposed a computation model in which we proved that halogen-oxygen vacancies are responsible for TiO$_2$ excitation under Vis irradiation. Moreover, the formation of oxygen vacancies on TiO$_2$ is equivalent to the occurrence of Ti^{3+} centers that, in consequence, leads to the creation of unpaired electrons, which could form donor levels in the electronic structure of TiO$_2$ [19]. Described in detail, in this computational model a surface complex between the halide anion and TiO$_2$ vacancy plays a central role. Unlike halide anions, both TiO$_2$ particles and 1-butylpirydynium cation do not absorb in the visible spectrum. Therefore, one might suspect that the presence of halide anions makes TiO$_2$ photoactive in the visible light. In order to prove this assumption, we employed the described in the literature OV in an anatase particle, i.e., Ti$_{35}$O$_{69}$ [20]. In Figure 5, the spin density originating from the two excess electrons associated with an oxygen vacancy are compared in Ti$_{35}$O$_{70}$ and in the same particle where the vacancy interacts with the halogen anion and oxygen molecule.

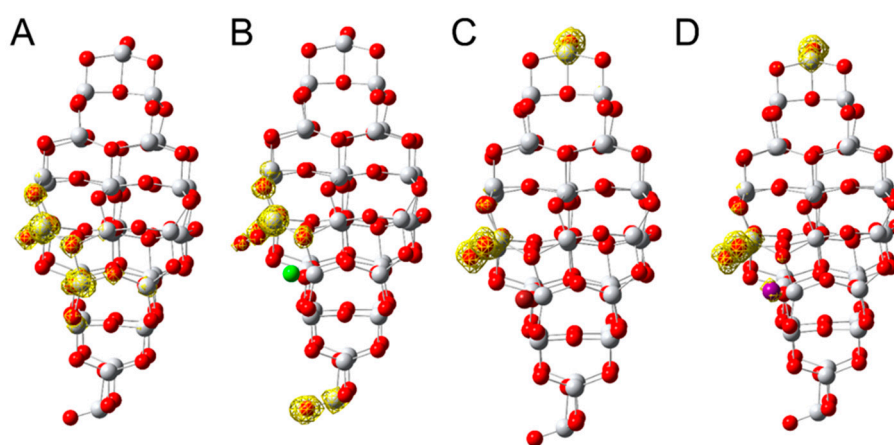**Figure 5.** Ti$_{35}$O$_{69}$ model of oxygen vacancy, (the oxygen vacancy formation for the depicted Ti$_{35}$O$_{69}$ structure amounts to 4.17 eV [20]), (**A**) without and (**B–D**) with oxygen and X$^-$ interacting with the system. Red and white spheres correspond to oxygen and titanium atoms while green, brown and violet spheres are chlorine (**B**), bromine (**C**) and iodine (**D**) atoms, respectively. The yellow meshes stand for spin density for isosurface of 0.002 e/(a.u)^3 calculated at the PM6 level—single electron (multiplicity equal to 3) is localized to each Ti^{3+} cation forming the vacancy (**A**) or is moved to the tip oxygen due to interaction with X$^-$ (**B**).

Due to this interaction spin density is partially transferred to the particle fragment distant to the position of the (OV)X$^-$···O$_2$ complex (see Figure 5; cf. A with B, C or D). Moreover, the excess electron is removed from the Ti^{3+} cation which interacts with the halogen anion that suggests the oxidation of titanium cation to Ti^{4+} due to complex formation. It is worth emphasizing that the halogen anions do not form stable complexes with O$_2$ in solution. For instance, the distance between the bromide anion and the closest of oxygen atom in the O$_2$ molecule amounts to as much as 4.19 Å, while the interaction energy is as low as 0.2 kcal/mol for the Br$^-$···O$_2$ system optimized at the PBE0/def2TZVP level and using the PCM model of water. Therefore, one can conclude that formation of the Br$^-$···O$_2$ complex, an indispensable condition for the photoinduced electron transfer between Br$^-$ and O$_2$, is negligible in solution. In contrast, interactions between an oxygen vacancy, Br$^-$ and O$_2$ make the distance between the halide anion and oxygen short enough to enable the photoinduced electron transfer to be efficient.

Indeed, regarding the abovementioned stabilization energy for the Br$^-$···O$_2$ complex, the interaction energy corresponding to the absorption of a halide anion and oxygen molecule on the oxygen vacancy is much larger. As indicated by the data gathered in Table S3, depending on the halide anion, this interaction energy spans the range from 46 to 60 kcal/mol. Interestingly, the absorption energies calculated for a larger cluster, Ti$_4$O$_{12}$, are within 2 kcal/mol identical with those for Ti$_2$O$_6$ (see Table S3), which suggests that already the smaller model should deliver reliable

results. Moreover, the gas phase interaction energies calculated at the PM6 level for the full $Ti_{35}O_{69}$ model (see Table S3) are similar to those obtained for the smaller models of oxygen vacancy. On the on hand, this fact confirms the validity of the Ti_2O_6 model and on the other hand shows that the local geometry of the vacancy being in the closest vicinity to the halide anion and oxygen decides on the adsorption characteristics.

The ground state spin distribution suggests, thus, that due to the formation of the abovementioned complex, the system becomes prepared for the excited state electron transfer between a halide anion and molecular oxygen. This observation prompted us to propose a simplified vacancy model (in order to enable more accurate DFT model to be employed) comprising just two titanium cations, Ti^{3+} (having an unpaired electron interacting with O_2 and Ti^{4+} interacting with X^-, see Figure 6).
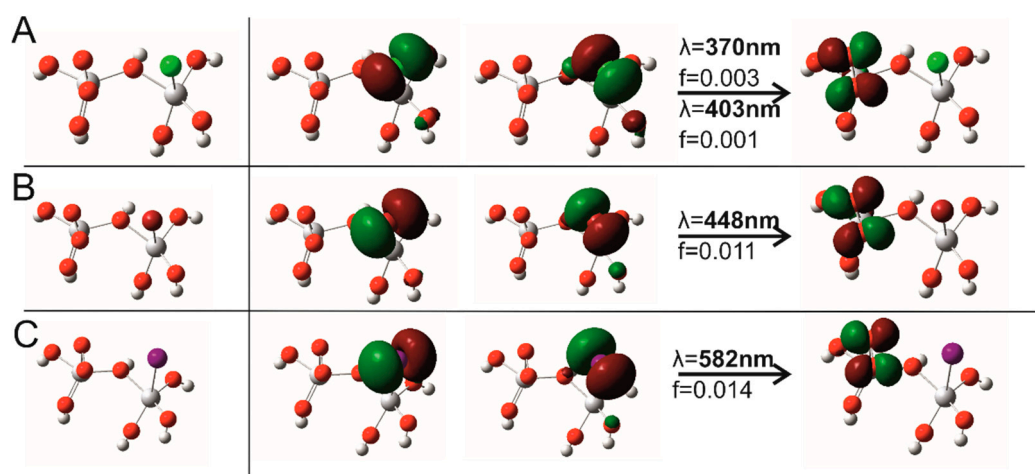

Figure 6. The simplified vacancy model (left) used for TD-DFT calculations, optimized with Cl^- (**A**), Br^- (**B**) and I^- (**C**) anions, respectively, and leading transitions in the long wavelength region of absorption with the wavelength and the oscillator strength shown (right).

In order to demonstrate that the cluster of Ti_2O_4 size properly describes the system under consideration we also analyzed Ti_4O_{12} (cut out from the $Ti_{35}O_{69}$ model of oxygen vacancy (see Figure 5) which is two times larger than the original one. The TD-DFT calculations for Ti_4O_{12}, performed at the PBE0/Def2TZVP/PCM level of theory, resulted in a similar transition to those obtained for Ti_2O_6. Namely, the leading transitions in the long wavelength region of absorption occur at similar values and similarly correspond to electron transfer from the halogen anion to the adsorbed oxygen molecule (see Figure S3 were the transitions in both clusters are compared).

For such models, constrained DFT optimizations were performed. Namely, the Ti_2O_6 fragment of a particle was fixed (a stiff structure of anatase particle does not deform because of the formation of a surface complex with oxygen and the X^- anion) at the geometry obtained by Kim et al. [20], whereas all degrees of freedom related to X^- and O_2 were fully optimized at the PBE0/Def2-TZVP level and the PCM model of water [21,22]. Then, the electronic transitions were obtained at the TD-PBE0/Def2-TZVP/PCM level. In the long wavelength region of absorption, the leading transitions (>90%, see Figure 6) correspond to the excitation of the electron from the lone pair in the halogen anion to the π^* orbital localized in the oxygen molecule ($nX^- \rightarrow \pi^*O_2$). These transitions were calculated at 370/403, 448 and 582 nm for the complexes containing Cl^-, Br^- and I^- anions, respectively (see Figure 6). This type of excitation transfers an electron form X^- to the adsorbed oxygen molecule. Since a monopole–monopole interaction between Ti^{4+} and X^-, a major force binding X^- to Ti^{4+}, does not exist in such an excited state, the transfer of the X atom to water is facilitated, which makes the formation of $O_2^{\bullet-}$ irreversible.

In order to confirm the theoretical calculations, the apparent quantum efficiency of the photocatalysts was estimated. The apparent quantum efficiency reflects the ratio of the rate of

the electron consumption from the initial rates of benzoquinone formation (first product of phenol oxidation) to the flux of incident photons. For each sample, the apparent quantum efficiency (AQE) was measured at three different wavelengths, i.e., at the absorption maxima predicted by the DFT model (403, 448 and 582 nm for Cl^-, Br^- and I^-, respectively, see Figure 6) and additionally for the wavelengths longer and shorter by 30 nm with respect to the mentioned above maxima. Additionally, the AQE for pristine TiO_2 was examined. The AQE for the TiO_2 samples modified with halide-based ionic liquids is presented in Table 3.

Table 3. Apparent quantum efficiency (AQE) of TiO_2 samples modified by ionic liquids containing halogen anions.

$TiO_2\_[BPy][Cl]$		$TiO_2\_[BPy][Br]$		$TiO_2\_[BPy][I]$	
λ * (nm)	AQE (%)	λ (nm)	AQE (%)	λ (nm)	AQE (%)
370	6.43	420	5.29	550	0.87
403	4.88	448	3.16	582	1.31
430	4.22	480	3.07	610	0.47

* λ—Excitation wavelength (nm).

In the case of the photocatalysts containing chloride or bromide anions, AQE decreases with the increasing wavelength, which is typical for titania [23,24]. Described in detail, the relatively high photoactivity of $TiO_2\_[Bpy][Cl]$ for wavelength of 370 nm (Table 3) resulted from: (i) the fact that pristine TiO_2, as a wide band-gap semiconductor, is excited itself mainly under the UV region of irradiation and, (ii) additionally from the existence of the absorbing complex at $\lambda = 370$ nm, which is consistent with theoretical studies (Figure 6). The activity of photocatalysts tested at longer wavelengths (403, 420, 430 nm (Table 3)) was mainly due to the existence of a surface complex, which was predicted by theoretical calculations. It is worth mentioning that pristine TiO_2 was still slightly photoactive under visible range of irradiation (see Figure S4). This might be due to existence of oxygen vacancies (Ti^{3+} states) or with the presence of impurities on the TiO_2 surface formed during the synthesis. Action spectra measurements of phenol photodegradation over pristine TiO_2 as well as IL-assisted TiO_2 are presented in Figure S4. However, the activity above 450 nm (Br^-/I^- modified samples) should be solely caused by the presence of halogen, since only defect-rich and modified (surface and doped) titania samples possess such activity. Interestingly, for the sample synthesized in the presence of iodide anion ([BPy][I]), the maximal AQE of 1.31% was measured at 582 nm (0.87% at 550 nm and 0.47% at 610 nm (see Table 2)), which agrees well with the results of our quantum chemical calculations (see Figure 6) and indicates the evident effect of iodide anion on the TiO_2 photoactivity. In case of such long wavelengths, the intrinsic activity of titania cannot affect the activity of $TiO_2\_[BPy][I]$.

Additionally, in order to gain insight into the ionic liquid mode of action, the thermal decomposition of 1-butylpirydium chloride under solvothermal reaction was investigated by using HPLC. The decomposition experiment was performed under the identical conditions as the synthesis of IL-TiO_2 samples i.e., 180 °C, 24 h. It was found that the decomposition efficiency of the [BPy][Cl] was 50% [25]. The HPLC results are consistent with the XPS analysis, namely Ti-Nx species formation (Table S2). On the basis of the XPS results, we can deduce that N atoms were probably introduced into the TiO_2 lattice during the solvothermal synthesis. Since nitrogen has a comparable atomic size as oxygen, small ionization energy and high stability, the N doping can be an effective way to enhance the absorption of TiO_2 under the visible range of irradiation. It is related to change in the banding structure of TiO_2 due to nitrogen atoms' substitution and formation of surface oxygen vacancies. More details about different ILs decomposition in the above mentioned conditions were described in our publication in which we developed computational methodology allowing for prediction properties of newly synthesized IL-TiO_2 materials before their synthesis [25].

3. Materials and Methods

3.1. Samples Preparation Method

The IL-assisted TiO$_2$ microparticles were synthesized by the procedure developed and optimized in our previous work [10]. Titanium(IV) butoxide (TBOT, Sigma-Aldrich, St. Louis, MO, USA) used as a precursor of TiO$_2$ was dissolved in an absolute ethanol (Avantor Performance Materials Poland S.A., Gliwice, Poland) with the purity 99.9%. Then, hydrochloric acid (Sigma-Aldrich, St. Louis, MO, USA) and distilled water were added. In the next step, the 1-butylpirydynium (Iolitec, Heilbronn, Germany) ionic liquid with different anions (chloride, bromide, iodide) was added in molar ratio 1:3 (IL:TBOT). The amount of IL added to the reaction system was selected based on our previous results [16]. The obtained reaction mixture was placed in a Teflon-lined stainless-steel autoclave and kept at 180 °C for 24 h. After the end of the set time, the reactor was cooled down at room temperature. The product was washed with ethanol (Avantor Performance Materials Poland S.A., Gliwice, Poland) and deionized water, dried at 50 °C for 12 h, and finally calcined at 200 °C for 2 h. For comparison, reference TiO$_2$ was synthesized using the same procedure without addition of IL.

3.2. Characteristic of the Material

The morphology (particle size and shape) of the IL-TiO$_2$ microparticles was measured by a scanning electron microscope (SEM, JEOL JSM-7610F, Jeol Ltd., Tokyo, Japan) working in a high vacuum mode. Powder X-ray diffraction (XRD) studies of the photocatalyst samples were carried out using a Rigaku MiniFlex 600 XRD system (Rigaku Corporation, Tokyo, Japan) equipped an X-ray generator with a copper target (operated at 40 kV and 40 mA). A Nicolet Evolution 220 UV-vis spectrophotometer (ThermoFisher Scientific, Waltham, MA., USA) was used to obtain the diffuse reflectance UV-vis absorption spectra of the samples, for which the baseline was performed using BaSO$_4$. The surface composition was analysed by X-ray photoelectron spectroscopy (XPS) using a PHI 5000 VersaProbe^{TM} spectrometer (ULVAC-PHI, Chigasaki, Japan) with monochromatic Al Kα irradiation (hν = 1486.6 eV) from an X-ray source operating at 100 μm spot size, 25 W and 15 kV. The high-resolution (HR) XPS spectra were recorded with the hemispherical analyser at the pass energy of 23.5 eV, the energy step size of 0.1 eV and the photoelectron take off angle 45° with respect to the surface plane. Casa XPS software (v.2.3.19, Casa Software Ltd, Wilmslow, United Kigdom) was used to evaluate the XPS data. The binding energy (BE) scale of all detected spectra was referenced by setting the BE of C 1s signal to 284.8 eV.

3.3. Photocatalytic Testes (Screening Tests)

To investigate the photocatalytic activity of the composites of TiO$_2$ prepared in the presence of IL, the decomposition rate of phenol (Avantor Performance Materials Poland S.A., Gliwice, Poland) 0.21 mmol·dm^{-3} in an aqueous solution was measured. The mixture of 0.125 g of the photocatalysts in 25 mL of phenol solution was stirred using a magnetic stirrer in a cylindrical reactor with a quartz window. The aeration of the suspension (5 dm^3/h) was maintained prior to and during the photocatalytic process. The photoirradiation was provided by a 1000 W Xenon lamp (6271H, Oriel), capable of emitting both the UV and visible light. For all measurements, an optical filter was used, with wavelengths λ > 420 nm. During the illumination, aliquots of the aqueous suspension with a volume of 1 cm^3 were successively sampled. Removal of the fine particles of the photocatalyst was performed by filtering the samples through a 0.2 μm syringe filter. To determine the phenol concentration, the colorimetric method (λ_{max} = 480 nm) was used with the UV-vis spectrophotometer (Nicolet Evolution 220, ThermoFisher Scientific, Waltham, MA., USA). The blind test (in the absence of the photocatalysts or illumination) proceeded the photocatalytic degradation runs. The absence of either the photocatalyst or illumination resulted in lack of phenol degradation.

3.4. Irradiations (Action Spectral Measurements)

Each photocatalyst powder (15 mg) was suspended in the aqueous solution (3.0 mL) of phenol (C_0 = 20 mg·L^{-1}) and placed in a rectangular quartz cell (10 mm^2 and 50 mm in height), then irradiated at monochromatic wavelengths for 60 min using a diffraction grating-type illuminator (Jasco, CRM-FD) equipped with a 300 W Xenon lamp (Hamamatsu, C2578-02). The light intensity was measured by an optical power meter (HIOKI 3664). The light intensity varied from 5.231 to 14.113 mW/cm^2 depending on the wavelength. During the experiments, the reaction mixtures were continuously stirred, and a portion (0.2 mL) of the reaction mixture was withdrawn every 20 min with a syringe, filtered (∅ = 0.2 μm, Whatman, Mini-UniPrep) to remove photocatalyst particles and subjected to a HPLC analysis. The HPLC Shimadzu LC-6A system (Shimadzu, Kyoto, Japan) was equipped with a WAKOSIL-II SC18 AR reversed-phase column (250 × 4.6 mm) and the UV detector (254 nm). A flow rate of a mobile phase composed of acetonitrile (29.5%), water (70%) and phosphoric acid (0.5%) was 1 mL·min^{-1}.

3.5. Computations

The TD-DFT (time-dependent density functional theory) calculations were performed with the use of PBE0 functional and Def2-TZVP basis set on the geometries optimized at the same level of theory. PBE0 functional [26] is known to produce reliable results [27] for the excited states while the Def2-TZVP basis set was chosen since it is available for all three halogens studied in the current work. The water environment was simulated by the PCM model [21,22]. All calculations were carried out with the Gaussian09 package (ver. D.01, Gaussian, Inc., Wallingford, CT, USA) [28].

4. Conclusions

In summary, based on our findings, we demonstrated that the improved, under visible irradiation, photoactivity of TiO$_2$ modified with the selected ILs, originates from the interactions of the IL's halogen anion (Cl$^-$/Br$^-$/I$^-$) and molecular oxygen with the TiO$_2$ surface. These interactions lead to the formation of a surface complex that allows photoinduced charge transfer (CT) to be accomplished. We concluded that TiO$_2$ enables the adsorption of halides on the oxygen vacancies. Based on our findings, we proposed a phenol photodegradation mechanism in which the O$_2{}^{\bullet-}$ radical anions are formed in the primary photochemical reaction. The latter process constitutes a photoinduced electron transfer (ET) between the halogen anion and adsorbed O$_2$. Indeed, using the TD-DFT method, we demonstrated the presence of electronic transition of significant oscillator strength at specific wavelength (370 and 403 nm for Cl$^-$, 448 nm for Br$^-$ and 582 nm for I$^-$) in the system comprising a model of OV and the adsorbed Cl$^-$/Br$^-$/I$^-$ and O$_2$ ((OV)X$^-$···O$_2$). The calculated wavelengths correspond well to the experimentally determined spectral region of the TiO$_2$ photoreactivity. Additionally, we concluded that the nitrogen doping can also take part in the mechanism of phenol decomposition under visible irradiation; however, the first mechanism likely dominates. In this regard, the mechanism of TiO$_2$ photoactivity enhancement is still unclear and needs further research, especially the experimental conformation. Explanation of the photodegradation mechanism is crucial to understand the mode of action of this materials and design new with improved activity.

Supplementary Materials: The following are available online at http://www.mdpi.com/2073-4344/10/4/371/s1, Figure S1. XPS HR spectra of Ti 2p of the TiO$_2$ photocatalysts modified with halide-based ionic liquids. Figure S2: Efficiency of phenol degradation under visible irradiation determined for the samples: TiO$_2$, TiO$_2$_[BPy][Cl], TiO$_2$_[BPy][I], TiO$_2$_[BPy][Br]. Figure S3: Two vacancy models (left) used for TD-DFT calculations (upper structure corresponds to the smaller model, Ti$_2$O$_6$, while the lower geometry, Ti$_4$O$_6$, to the large one), optimized with interacting oxygen and Cl$^-$ (A), Br$^-$ (B) and I$^-$ (C) anions respectively along with leading transitions in the long wavelength region of absorption with the wavelength and the oscillator strength shown on the arrows (right). Figure S4: Action spectra for the photocatalytic degradation of phenol in the presence of pristine TiO$_2$ and TiO$_2$ obtained using ionic liquid containing various anions., Table S1: Lattice parameters and average crystallite size of the TiO$_2$_[BPy][X] photocatalysts., Table S2: Elemental composition (in at. %) and chemical characters of titanium, oxygen and carbon states in the surface layer of TiO$_2$ and [BPy][Cl], [BPy][Br], [BPy[[I] IL-modified TiO$_2$ particles, evaluated by XPS analysis. Table S3. Adsorption energies (E_a) of halogen ion and molecular oxygen on the

Ti$_{35}$O$_{69}$, Ti$_2$O$_6$ and Ti$_4$O$_{12}$ clusters calculated at the PM6 or PBE0/Def2TZVP/PCM level of theory. The adsorption energy was estimated as the difference between the energy of the complex and the sum of the energies of the isolated cluster, halide anion and molecular oxygen.

References

1. Yun, E.-T.; Yoo, H.-Y.; Kim, W.; Kim, H.-E.; Kang, G.; Lee, H.; Lee, S.; Park, T.; Lee, C.; Kim, J.-H.; et al. Visible-light-induced activation of periodate that mimics dye-sensitization of TiO2: Simultaneous decolorization of dyes and production of oxidizing radicals. *Appl. Catal. B Environ.* **2017**, *203*, 475–484. [CrossRef]

2. Samsudin, E.M.; Hamid, S.B.A.; Juan, J.C.; Basirun, W.J.; Centi, G. Enhancement of the intrinsic photocatalytic activity of TiO2 in the degradation of 1,3,5-triazine herbicides by doping with N,F. *Chem. Eng. J.* **2015**, *280*, 330–343. [CrossRef]

3. Park, Y.; Singh, N.J.; Kim, K.S.; Tachikawa, T.; Majima, T.; Choi, W. Fullerol–Titania Charge-Transfer-Mediated Photocatalysis Working under Visible Light. *Chem. Eur. J.* **2009**, *15*, 10843–10850. [CrossRef]

4. Lamba, R.; Umar, A.; Mehta, S.K.; Kansal, S.K. Enhanced visible light driven photocatalytic application of Ag2O decorated ZnO nanorods heterostructures. *Sep. Purif. Technol.* **2017**, *183*, 341–349. [CrossRef]

5. Gołąbiewska, A.; Zielińska-Jurek, A.; Zaleska, A. Characterization of TiO$_2$ modified with bimetallic Ag/Au nanoparticles obtained in microemulsion system. *J. Adv. Oxid. Technol.* **2012**, *15*, 71–77.

6. Liu, H.; Liang, Y.; Hu, H.; Wang, M. Hydrothermal synthesis of mesostructured nanocrystalline TiO$_2$ in an ionic liquid–water mixture and its photocatalytic performance. *Solid State Sci.* **2009**, *11*, 1655–1660. [CrossRef]

7. Hardacre, C.; Holbrey, J.D.; McMath, S.E.J.; Bowron, D.T.; Soper, A.K. Structure of molten 1,3-dimethylimidazolium chloride using neutron diffraction. *J. Chem. Phys.* **2003**, *118*, 273–278. [CrossRef]

8. Łuczak, J.; Paszkiewicz, M.; Krukowska, A.; Malankowska, A.; Zaleska-Medynska, A. Ionic liquids for nano- and microstructures preparation. Part 1 Properties and multifunctional role. *Adv. Colloid Interface Sci.* **2016**, *230*, 13–28. [CrossRef] [PubMed]

9. Łuczak, J.; Paszkiewicz, M.; Krukowska, A.; Malankowska, A.; Zaleska-Medynska, A. Ionic liquids for nano- and microstructures preparation. Part 2: Application in synthesis. *Adv. Colloid Interface Sci.* **2016**, *227*, 1–52. [CrossRef] [PubMed]

10. Paszkiewicz, M.; Łuczak, J.; Lisowski, W.; Patyk, P.; Zaleska-Medynska, A. The ILs-assisted solvothermal synthesis of TiO2 spheres: The effect of ionic liquids on morphology and photoactivity of TiO$_2$. *Appl. Catal. B Environ.* **2016**, *184*, 223–237. [CrossRef]

11. Gołąbiewska, A.; Checa-Suárez, M.; Paszkiewicz-Gawron, M.; Lisowski, W.; Raczuk, E.; Klimczuk, T.; Polkowska, Ż.; Grabowska, E.; Zaleska-Medynska, A.; Łuczak, J. Highly Active TiO$_2$ Microspheres Formation in the Presence of Ethylammonium Nitrate Ionic Liquid. *Catalysts* **2018**, *8*, 279. [CrossRef]

12. Ramanathan, R.; Bansal, V. Ionic liquid mediated synthesis of nitrogen, carbon and fluorine-codoped rutile TiO$_2$ nanorods for improved UV and visible light photocatalysis. *RSC Adv.* **2015**, *5*, 1424–1429. [CrossRef]

13. Yu, J.; Li, Q.; Liu, S.; Jaroniec, M. Ionic-Liquid-Assisted Synthesis of Uniform Fluorinated B/C-Codoped TiO2 Nanocrystals and Their Enhanced Visible-Light Photocatalytic Activity. *Chem. Eur. J.* **2013**, *19*, 2433–2441. [CrossRef]

14. Łuczak, J.; Paszkiewicz-Gawron, M.; Długokęcka, M.; Lisowski, W.; Grabowska, E.; Makurat, S.; Rak, J.; Zaleska-Medynska, A. Visible light photocatalytic activity of ionic liquid-TiO$_2$ spheres: Effect of the ionic liquid's anion structure. *ChemCatChem* **2017**, *9*, 4377–4388. [CrossRef]

15. Qi, L.; Yu, J.; Jaroniec, M. Enhanced and suppressed effects of ionic liquid on the photocatalytic activity of TiO$_2$. *Adsorption* **2013**, *19*, 557–561. [CrossRef]

16. Paszkiewicz-Gawron, M.; Długokęcka, M.; Lisowski, W.; Paganini, M.C.; Giamello, E.; Klimczuk, T.; Paszkiewicz, M.; Grabowska, E.; Zaleska-Medynska, A.; Łuczak, J. Dependence between Ionic Liquid Structure and Mechanism of Visible-Light-Induced Activity of TiO$_2$ Obtained by Ionic-Liquid-Assisted Solvothermal Synthesis. *ACS Sustain. Chem. Eng.* **2018**, *6*, 3927–3937. [CrossRef]

17. Ratke, L.; Voorhees, P.V. *Growth and Coarsening: Ostwald Ripening in Material Processing*; Springer Science & Business Media: Berlin/Heilderberg, Germany; New York, NY, USA, 2002.

18. Gołąbiewska, A.; Paszkiewicz-Gawron, M.; Sadzińska, A.; Lisowski, W.; Grabowska, E.; Zaleska-Medynska, A.; Łuczak, J. Fabrication and photoactivity of ionic liquid–TiO$_2$ structures for efficient visible-light-induced photocatalyticdecomposition of organic pollutants in aqueous phase. *Beilstein J. Nanotechnol.* **2018**, *9*, 580–590. [CrossRef]

19. Pan, X.; Yang, M.-Q.; Fu, X.; Zhang, N.; Xu, Y.-J. Defective TiO$_2$ with oxygen vacancies: Synthesis, properties and photocatalytic applications. *Nanoscale* **2013**, *5*, 3601–3614. [CrossRef]

20. Kim, S.; Ko, K.C.; Lee, J.Y.; Illas, F. Single oxygen vacancies of (TiO2)35 as a prototype reduced nanoparticle: Implication for photocatalytic activity. *Phys. Chem. Chem. Phys.* **2016**, *18*, 23755–23762. [CrossRef]

21. Cossi, M.; Barone, V.; Cammi, R.; Tomasi, J. Ab Initio Study of Solvated Molecules: A New Implementation of the Polarizable Continuum Model. *Chem. Phys. Lett.* **1996**, *255*, 327–335. [CrossRef]

22. Miertus, S.; Scrocco, E.; Tomasi, J. Electrostatic interaction of a solute with a continuum. A direct utilizaion of AB initio molecular potentials for the prevision of solvent effects. *Chem. Phys.* **1981**, *55*, 117–129. [CrossRef]

23. Reszczyńska, J.; Grzyb, T.; Sobczak, J.W.; Lisowski, W.; Gazda, M.; Ohtani, B.; Zaleska, A. Visible light activity of rare earth metal doped (Er^{3+}, Yb^{3+} or Er^{3+}/Yb^{3+}) titania photocatalysts. *Appl. Catal. B Environ.* **2015**, *163*, 40–49. [CrossRef]

24. Reszczyńska, J.; Grzyb, T.; Sobczak, J.W.; Lisowski, W.; Gazda, M.; Ohtani, B.; Zaleska, A. Lanthanide co-doped TiO$_2$: The effect of metal type and amount on surface properties and photocatalytic activity. *Appl. Surf. Sci.* **2014**, *307*, 333–345. [CrossRef]

25. Rybińska-Fryca, A.; Mikołajczyk, A.; Łuczak, J.; Paszkiewicz-Gawron, M.; Paszkiewicz, M.; Zaleska-Medynska, A.; Puzyn, T. How thermal stability of ionic liquids lead to more efficient TiO$_2$-based nanophotocatalysts: Theoretical and experimental studies. *J. Colloid Interface Sci.* **2020**, in press.

26. Adamo, C.; Barone, V. Toward reliable density functional methods without adjustable parameters: The PBE0 model. *J. Chem. Phys.* **1999**, *110*, 6158–6170. [CrossRef]

27. Jacquemin, D.; Wathelet, V.; Perpète, E.A.; Adamo, C. Extensive TD-DFT Benchmark: Singlet-Excited States of Organic Molecules. *J. Chem. Theory Comput.* **2009**, *5*, 2420–2435. [CrossRef]

28. Frisch, M.J.; Trucks, G.W.; Schlegel, H.B.; Scuseria, G.E.; Robb, M.A.; Cheeseman, J.R.; Scalmani, G.; Barone, V.; Mennucci, B.; Petersson, G.A.; et al. *Gaussian 09, ver. D.01.*; Gaussian, Inc.: Wallingford, CT, USA, 2009.